Presented at the 19th EU PVSEC, June 2004, Paris 2.CV.2.34

SOLAR CELLS ON N-TYPE MULTICRYSTALLINE SILICON WAFERS BY INDUSTRIAL PROCESSING TECHNIQUES

C.J.J. Tool[1], H.C. Rieffe[1], R. Kinderman[1], R. Kopececk[2], K. Wambach[3], L.J. Geerligs
[1]ECN Solar Energy, PO Box 1, NL-1755 ZG Petten, The Netherlands
Tel: +31 224 564135, fax: +31 224 568214, email: tool@ecn.nl
[2]University of Konstanz, Jacob-Burckhardt-Str. 29, D-78464 Konstanz, Germany
[3]Deutsche Solar, Alfred-Lange Str. 18, D-09599 Freiberg/Sachsen, Germany

ABSTRACT: n-type silicon can be an interesting material to reduce the expected silicon shortage. We are developing an industrial process sequence of n-type silicon. We report improvements of emitter processing and implementation of a SiN_x ARC which resulted in an increase of the efficiency from about 5 % to over 12 %. Further optimization of the front side paste and the firing conditions can increase the efficiency to 14 %.
Keywords: n-type, multi-crystalline, doping

1 INTRODUCTION

It is generally accepted that within one or two years crystalline silicon PV technology will suffer from a feedstock problem [1,2]. At the same time a large amount of highly doped n-type silicon is available as byproduct from the electronic industry. At the moment, this material is not suitable for the PV industry because the n-type dopant levels are too high and no suitable industrial solar cell processing sequences are available for multi-crystalline n-type material.

Deutsche Solar has started investigations into purifying the highly doped n-type material to make it suitable for PV applications. At ECN we are developing industrial processing sequences for this n-type material, while UKON does materials characterization and high efficiency processing to reveal the potential of the material. In this work we report on the industrial type solar cell processing; the work on an alternative type processing with a rear side emitter and the work on the properties of the material are presented in other papers at this conference [3, 4].

An additional motivation for the development of an industrial processing sequence for n-type silicon is the extremely high lifetimes observed in the material. It seems that n-type silicon is less sensitive to metallic impurities [5, 6], which makes n-type silicon attractive as a potential high efficiency material.

2 EXPERIMENTAL

Because no purified n-type material was available at the beginning of the project, we used multi crystalline wafers made by Deutsche Solar from a blend of highly doped n-type silicon with virtually undoped silicon. Ingots were grown in an industrial HEM furnace, and wire sawn to about 300 µm thick wafers.

The reference processing sequence consisted of an NaOH saw damage etch which removed about 25 µm, followed by boron emitter diffusion from a spin-on dopant source in an IR-heated belt furnace. After boron-glass removal the so called Boron Rich Layer (BRL) was removed by thermal oxidation in a belt furnace. This was followed by a phosphorous rear side diffusion to passivate the surface with a phosphorous Back Surface Field (P-BSF) also in an IR heated belt furnace. During P-BSF diffusion the B-emitter was protected by a capping layer to prevent compensation of the B-emitter by phosphorous via the gas phase. Edge isolation was done by grinding. Finally an RPECVD SiN anti-reflection coating (ARC) was applied and the rear and front contacts were screen printed and co-fired through the SiN in an IR-heated belt furnace. Because the rear side is passivated by a phosphorous BSF, an open H-pattern metallisation is used at the rear. Topsil PV-FZ n-type wafers [7] were processed as reference material.

From all cells the IV characteristic was measured according to ASTM-E948, while from selected cells the spectral response and reflection was measured to obtain the internal quantum efficiency (IQE). Both front and rear illumination has been used in the spectral response measurements which was possible because we used an open rear side metallisation.

In this work the influence of the boron source, the diffusion temperature and the BRL removal sequence are reported.

3 RESULTS AND DISCUSSION

3.1 Boron diffusion sources

Five different boron diffusion sources have been applied, 2 home made spin-on liquids (spin-on 1 and 2), 1 commercially available spin-on liquid (spin-on 3) and 2 commercially available boron pastes. Table I shows the average IV characteristics of the resulting mc-Si cells.

Table I: Average IV characteristics using various boron sources on 156 cm^2 mc-Si cells.

source	Jsc mA/cm^2	Voc mV	FF %	eta %	R_{serie} $\Omega.cm^2$	R_{shunt} $\Omega.cm^2$
spin-on 1	30.0	541	66	10.7	1.7	550
spin-on 2	30.2	541	68	11.1	1.7	1200
spin-on 3	28.8	542	67	10.5	1.7	600
paste-1	27.5	491	66	8.9	1.7	850
paste-2[a]	28.0	534	66	9.8	1.7	600
BBr_3[b]	28.2	530	58	8.9		

[a]: 3 out of 6 cells were excluded; $J_{sc} < 1$ mA/cm^2
[b]: for comparison only; not on neighbor wafers; 100 cm^2 cell area

From Table I it is clear that the spin-on dopants give the best cell results. Although the IV characteristics using paste-2 are comparable to the spin-on dopants we observed a large variation in the emitter sheet resistivity and 3 out of the 6 cells had to be excluded from the analysis because they did not produce any current.

The IQE measurements revealed that the boron source used has a large influence on the minority carrier

lifetime of the bulk. This is most obvious from Figure 1 which shows the IQE measured from the rear side of the cells. Also shown are rear side illuminated IQE-curves calculated with PC1D for n-type cells with a bulk minority carrier diffusion length of 20, 50, 125 and 200 µs respectively. It is obvious that the bulk is deteriorated by the commercial boron sources; the best bulk lifetimes are observed for the two home made spin-on liquids.

Although spin-on liquid 2 gives the highest efficiency and highest bulk diffusion length, we decided to use spin-on liquid 1 as a reference material in the process variations (section 3.2) and firing through (section 3.3) because spin-on liquid 2 is not stable in time.

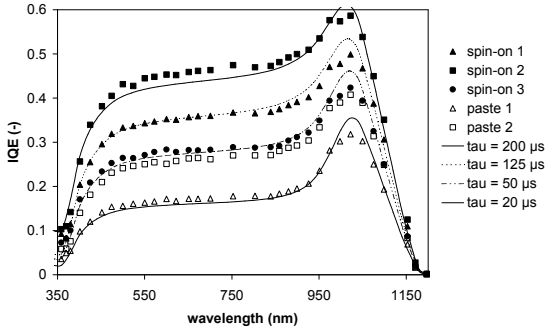

Figure 1: Rear side IQE; lines are calculated with PC1D for minority carrier lifetimes indicated in the legenda. IQE measurements have been performed on neighbouring cells. IQE of BBr_3 cell is not included because it is not a neighbor cell.

In Table II the major impurities of the boron sources measured with Atomic Absorption Spectroscopy (AAS) are summarized. It is not obvious from this table which impurity is responsible for the decreased minority carrier diffusion length. Ti is probably the interfering impurity in the pastes; while Na could be the cause of the degradation in spin-on 3. The boron sources contain a substantial amount of Fe, but the high lifetimes observed with spin-on source 1 and 2 confirm that Fe is not responsible for the low bulk quality. Fe is both gettered during phosphorous - BSF formation and n-type silicon is inherent insensitive to Fe impurities [5].

For comparison the results of cells processed with a BBr_3 tube furnace emitter are also shown in Table I. Although no neighbor wafers were used for this group, the results indicate that the low V_{oc} does not result from impurities in the boron source. Also FZ wafers have been processed showing comparable IV characteristics. This indicates that the cell performance is limited by the processing sequence and not by the materials properties which are known to be good [4]. That high efficiency n-type cells can be made from this material is shown on a small area by Libal et al. [8].

Table II: Major impurities in the boron sources as determined with AAS in ppm.

	Fe	Mo	Ti	Sn	other
det. limit	0.2	0.04	0.03	0.08	
spin-on 1	0.85	0.16	-	0.51	Ga: 0.36 Sc: 0.02
spin-on 2	0.4	0.1	-	0.34	Sc: 0.02
spin-on 3	0.62	0.06	-	-	Zn: 0.69 Na: 250
paste 1	2.1	0.06	0.18	0.34	Na: 16 Ca: 1.5
paste 2	0.8	0.06	0.29	0.63	Zn: 0.63 Pb: 2.3

-: below detection limit

3.2 process variations

To further investigate the influence of the emitter processing, we varied the diffusion temperature and the BRL removal method. To improve Voc and increase the shunt resistance (see section 3.4) we increased the diffusion temperature to obtain a more heavily doped emitter. The heavier diffusion resulted in a sheet resistivity of about 45 ohm/sq, compared to about 80 ohm/sq for the reference diffusion process.

The BRL is normally removed by a thermal oxidation in a belt furnace followed by an HF-dip. Impurities from the belt can then diffuse into the cell, so normally the P-BSF diffusion is performed after the oxidation to getter these impurities. In this comparison the BRL oxidation was performed after the P-BSF diffusion to increase the boron diffusion without increasing the thermal budget. As an alternative to thermal oxidation of the BRL, chemical oxidation of the BRL has also been tested.

The average values of the IV characteristics are given in Table III. Neighbor wafers over the groups have been used.

Table III: IV characteristics for various BRL removal sequences; average of 8 cells per group. Cell area is 156 cm^2

	Jsc mA/cm^2	Voc mV	FF %	η %	R_{seriss} $\Omega \cdot cm^2$	R_{shunt} $\Omega \cdot cm^2$
thermal oxidation	26.5	506	57	7.7	1.1	80
high T diffusion	26.0	540	69	9.7	0.9	350
chemical oxidation	25.8	532	55	7.5	2.5	150

Both the heavier diffusion and the chemical BRL removal increases the V_{oc} of the cell compared to the normal thermal oxidation process. The low FF in the chemical removal scenario is related to a high series resistance. Although the cells were hydrophobic after the BRL removal possibly the BRL was not fully removed resulting in an increased contact resistance. The increased FF for the high T diffusion cells result both from a decreased contact resistance (lower R_{series}) and an increased shunt resistance.

The front side IQE of both alternative processing schemes reveal a large decrease in the red response indicating a bulk deterioration compared to the reference scenario (Figure 2). For the high T diffusion scenario, this deterioration probably results from the higher diffusion temperature. The decreased red response in the chemical removal scenario is not understood. One reason could be a reduced bulk passivation because the

remaining BRL could have hindered the H-diffusion into the bulk. However, in additional experiments (section 3.3) no bulk passivation is observed in the reference scenario either.

The blue response is increased in both scenarios Figure 2 indicating an increase in the front surface passivation of the cells. The higher V_{oc} probably results from this increased passivation, although an increased blue response not always result in an increased V_{oc} (section 3.4)

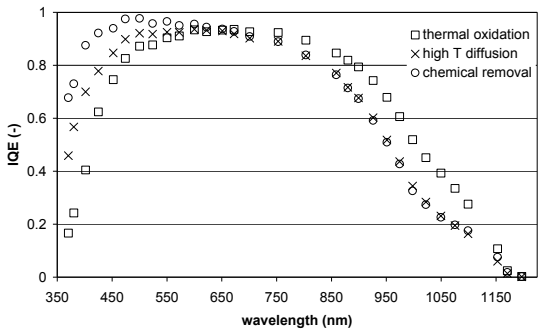

Figure 2: Front side iluminated IQE for various process scenarios.

3.3 bulk and surface passivation

On p-type wafers, hydrogen from the SiN ARC can be used for bulk passivation and front surface passivation. To realize the passivation, the coating has to be applied on a clean surface and a short thermal anneal is necessary. In an industrial processing sequence, this is achieved by applying the SiN before contact firing [9]. To investigate the passivating properties of a SiN coating on n-type cells, we compared the firing through processing sequence (denoted FT) with a sequence in which contact firing is performed before SiN deposition (the reversed scenario: RS) on neighbor mc-Si wafers and FZ wafers. In Table IV the IV characteristics of the cells are given. The metallisation area (A_{metall}) varied considerable from cell to cell, therefore the current density for the open cell area is given as $J_{open\ area}$ in column 4.

Table IV: IV-characteristics for RS and FT for both multi-crystalline (mc) and float zone (FZ) cells.

	A_{metall} %	J_{sc} mA/cm^2	$J_{open\ area}$ mA/cm^2	V_{oc} mV	FF %	η %
mc-1-RS	23.0	24.9	32.4	531	73.5	9.7
mc-1-FT	12.5	28.2	32.2	523	69.4	10.2
mc-2-RS	20.0	25.2	31.4	535	75.0	10.1
mc-2-FT	12.5	28.6	32.6	530	70.2	10.6
FZ-RS	20.8	26.2	33.0	534	73.7	10.3
FZ-RS	18.6	26.9	33.0	538	74.1	10.7
FZ-FT	12.5	29.5	33.7	529	54.7	8.5
FZ-FT	11.4	29.9	33.7	530	63.6	10.1

The lower FF in the FT scenario results from a higher series resistance, partly due to the lower metallisation area, and partly due to a higher contact resistance. The FT scenario results in 2 % increase of the open area current density and a 1 % decrease of the V_{oc} for both the FZ and the mc-Si cells. In Figure 3 the front side illuminated IQE of an mc-Si neighbor set and an Fz set is shown. For both type of materials, the blue response is substantially increased by the FT scenario, indicating that the front surface is passivated by the SiN coating.

No increase of the IQE is observed for wavelengths above 800 nm in the FT scenario. This indicates that the no bulk passivation is observed for the FT scenario. Actually a slight decrease is observed.

PC1D modeling of the IQE indicates that the FT scenario results in an effective front surface recombination (S_{fron}) of about 2.10^5 cm/s. Compared to an unpassivated front surface ($S_{fron} = 10^7$ cm/s), PC1D predicts a current gain of about 4.5 % compared to the 2 % current gain observed. Also, the V_{oc} should increase instead of decrease. The observed slight decrease in bulk quality is too small to explain the difference.

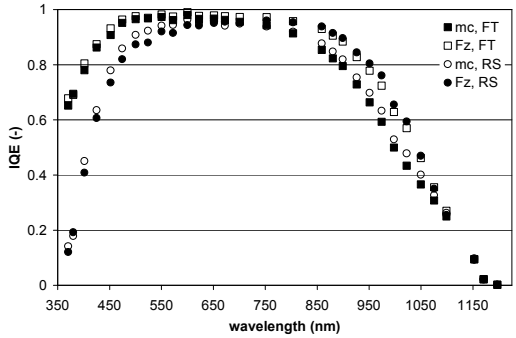

Figure 3: Front side illuminated IQE of FZ and multi-crystalline (mc) cells for both the firing though (FT) and reversed scenario (RS).

3.4 resistance losses

All produced cells suffer from resistance losses. The cells have typical series resistances of 1.7 Ωcm^2 and typical shunt resistances of 100-1000 Ωcm^2 as estimated from fits to the second diode model (e.g. Table I).

Table V: Influence of resistance losses on cell efficiency; using an optimized metallisation pattern. Cell area is 156 cm^2.

	ρ_{line} Ω/cm	R_{shunt} Ω.cm^2	J_{sc} mA/cm^2	V_{oc} mV	FF %	η %
exp.[a]	0.9[b]	300	30.4	549	68.7	11.4
modeling	0.9	300	30.4	548	68.7	11.4
- line	0.3[c]	300	31.3	549	71.9	12.4
- shunt	0.3	3000	31.5	550	74.5	12.9

[a]: cell from group spin-on 1 Table I
[b]: line width = 180 µm; finger spacing = 2 mm
[c]: line width = 120 µm; finger spacing = 2.5 mm

The influence of the series and shunt resistance on the IV characteristics has been estimated using the pattern optimization program developed by Burgers [10]. We did not perform a pattern optimization, but fixed the metallization pattern. As a starting point we used the second diode parameters of the cell. The output of the calculation is in good agreement with the measured cell results (see first 2 rows in Table V). Calculations using the pattern and conductivity of our normal screen printed silver grid results in an efficiency increase of 1 % absolute (row 3 Table V). The current gain results from the lower metallization area. Increasing the shunt resistance increases the efficiency by an additional 0.5 % absolute (last row Table V) due to an increase in the fill factor.

The series resistance originates from the metal used in the firing through process. To reveal the origin of the low shunt resistance, lock-in thermography has been

performed. In Figure 4 a typical example of a thermograph is shown. This thermograph reveales that three different shunt paths can be distinguished.

Edge shunt (A in Figure 4) could occur because the boron emitter is compensated at the edges during phosphorous BSF diffusion. The use of a capping layer reduced the edge shunt substantially, but it does not completely prevent it. Although the remaining cause of the edge shunt is not fully understood, most likely it is related to the spinning process used for applying both the boron and the phosphorous source. This shunt is removed by removing about 1 cm at each side of the cell by laser scribing and breakage.

The use of a paste capable to perform a firing through processing sequence, results in shunt paths underneath the busbar (B in Figure 4). Probably a firing optimization in combination with a heavier diffusion can overcome this problem.

The third shunt path (C in Figure 4) occurs randomly at spots on the surface. We do not understand the cause, but it is not correlated to the metallisation.

Besides type B shunt, the use of aluminum-containing silver metallization also results in an increase of the series resistance in the cells. The specific resistivities of the fired Ag/Al paste depends on the firing condition and varies between 10-25 μΩ.cm. For standard silver paste, the specific resistivity is 2.5 μΩ.cm and is almost independent of the firing conditions.

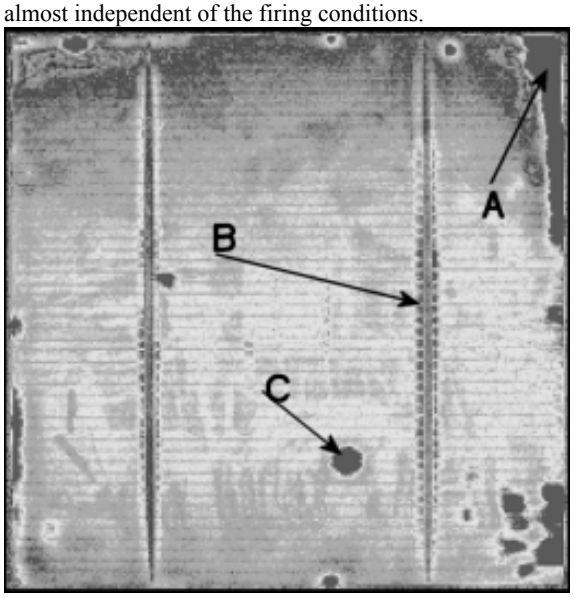

Figure 4: Thermography of n-type cell using spin-on 1; three typical shunt areas are indicated: A: edge shunt; B: busbar shunt; C: local shunt. R_{shunt} = 500 Ω.cm^2.

4 CONCLUSION

A careful choice of the boron diffusion source can have a tremendous effect on the bulk quality of the produced cells. The commercially available sources tested here contain too many impurities which results in a considerable bulk degradation.

The blue response of the cells can be increased by optimization of the emitter procedure (including BRL removal) and a firing-through scenario.

The use of a better metallization could increase the efficiency of the cells by about 2 % absolute.

Figure 5 shows the development in the efficiencies realized in this work over the past year using industrial processing schemes. Although the highest efficiency is well behind the 15+ % of p-type processing, the trend is promising.

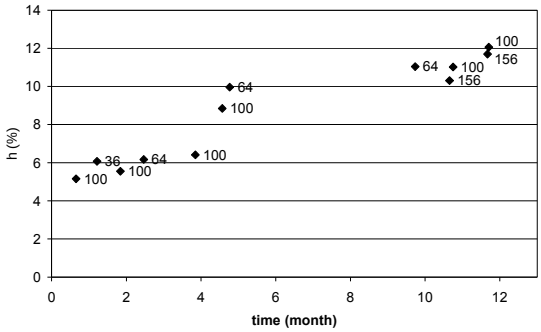

Figure 5: Efficiency development using industrial processing sequences during the past year. Value near the symbol indicates cell area in cm^2.

ACKNOWLEDGEMENT

We thank Joris Libal (University of Konstanz) for performing the BBr_3 diffusion on our samples.

This work is carried out as a part of the NESSI project funded by the European Commision's FP5 Energie R&D programme (contract number ENK6-CT2002-00660).

REFERENCES

[1] M. Schmela, Photon International, 4 (2004) 3.
[2] 1st Solar Silicon Conference, 22 April 2004, Munich.
[3] T. Buck, et al., Low cost p^+nn^+-type back juntion solar cells by screen printing technique on Cz and mc-Si material, this conference.
[4] J. Libal, et al., Properties of n-type multycrytslline silicon: lifetime, gettering and H-passivation, this conference.
[5] D. Macdonald, L.J Geerligs, Recombination activity of iron and other transition metals in p- and n-type crystlline silicon, this conference.
[6] A. Cuevas, M.J. Kerr, C. Samundsett, F. Ferrazza and G. Coletti, Appl. Phys. Lett, (2002), 81(26), 4952-4954.
[7] J. Vedde, T. Clausen, L. Jensen, Proc 3th WCPEC, Osaka 2003, 4O-D7-03
[8] J. Libal, private communication; to be published
[9] S. Winderbaum, A.J. Leo, S.P. Shea, T.D. Koval and B. Kumar, Proc 3th WCPEC, Osaka 2003, 4P-A8-80.
[10] A.R. Burgers, J.A. Eikelboom, Proc. 26th IEEE PVSC, Anaheim 1997, 219-222.